Robotics and Autonomous Systems 61 (2013) 13–24

Contents lists available at SciVerse ScienceDirect

Robotics and Autonomous Systems

journal homepage: www.elsevier.com/locate/robot

Systematic kinematics analysis and balance control of high mobility rovers over rough terrain

Mahmoud Tarokh [a,*], Huy Dang Ho [a], Antonios Bouloubasis [b]

[a] Department of Computer Science, San Diego State University, San Diego, CA 92182, USA
[b] GO Science Ltd, 1375 Aztec West, Park Avenue, Bristol, BS32 4SB, England, United Kingdom

ARTICLE INFO

Article history:
Received 16 August 2010
Received in revised form
16 September 2011
Accepted 26 September 2012
Available online 17 October 2012

Keywords:
Rover kinematics
Balance control
High mobility rovers

ABSTRACT

The paper proposes a systematic method for kinematics modeling, analysis and balance control of a general high mobility wheeled rover traversing uneven terrain. The method is based on the propagation of position and orientation velocities starting from the rover reference frame and going through various joints and linkages to the wheels. The concept of an extended DH table is introduced for rovers and mobile robots, and equations of the motion are set up in a compact form. Actuation kinematics and balance control are formulated for rovers traversing bumpy terrains. To illustrate the proposed kinematics modeling and balancing, the method is applied to a high mobility rover and simulation results with various terrains are presented.

1. Introduction

Rovers with high mobility mechanisms are capable of traversing rough terrain and adapting their configurations to the changing terrain topology. They are being used increasingly in diverse applications such as terrestrial and planetary explorations [1,2], forestry [3], agriculture [4], mining industries [5], defense and hazardous material handling and de-mining [6]. Rovers with active suspension systems are capable of modifying and adjusting their suspension linkages and joints so as to change their center of mass to avoid tip over while traversing rough and inclined terrain [7,8].

Research efforts on kinematics modeling have been mainly limited to simple mobile robots moving on flat terrain [9–11]. Recently attention has been directed towards high mobility rovers. A study of the kinematics of a particular rover is reported in [12]. In a recent paper [13], we developed a full kinematics model of articulated rovers and provided analysis of such rovers. Reusable kinematics models and algorithms for manipulators and vehicles are reported in [14] within the framework of object-oriented software. The work reported in [15] employs a simple kinematics model and a state observer to estimate rover position/orientation velocities. A Kalman filter approach is proposed in [16,17] to estimate wheel contact angles for traction control. A method for ensuring the stability of articulated rovers is discussed in [18]. Wheel driving force and tip-over stability are also considered in [19] where a scheme is proposed to utilize the rover center of mass in order to aid in traversing rough terrain.

It is well known that a systematic and universal approach exists for kinematics modeling of robot manipulators. In this approach, a so called Denavit–Hartenberg (DH) table is set up which specifies four parameters for forming a transformation matrix for each frame in the kinematics chain. The transformation matrices are cascaded (multiplied) to find the aggregate transformation between a base frame and a desired frame in the kinematics chain. Using this aggregate transformation matrix, the position and orientation of the desired frame, e.g. end-effector, are extracted and expressed in terms of joint/link values. However, such a methodology does not exist for articulated rovers due to the complexity of the rover suspension mechanism, closed chain kinematics, motion over uneven terrain, existence of both actuated and compliant joints/links, and unmeasurable quantities such as various slips. The goal of this paper is to propose a systematic method for developing full kinematics models for motions over uneven terrain of general articulated wheeled rovers. The proposed approach is superior to our earlier work [13] in the sense that it is applicable to a more general class of rovers, can be implemented via symbolic or numeric manipulation and is suitable for direct computer implementation. Furthermore, in this paper we include a method for balance control and augment it with the rover kinematics to ensure that the rover is stable and the tip over is prevented.

* Corresponding author.
E-mail addresses: tarokh@sdsu.edu, tarokh@cs.sdsu.edu (M. Tarokh).

0921-8890/$ – see front matter © 2012 Elsevier B.V. All rights reserved.
doi:10.1016/j.robot.2012.09.010

2. Kinematics modeling and analysis

A high mobility wheeled rover is defined as a rover that consists of a main body connected to a set of wheels via a set of linkages and joints that are adjusted so as to enable it to traverse the uneven terrain. The joints and linkages change either passively or actively. Active linkages and joints have actuators through which their values can be controlled, whereas passive ones change their values to comply with the terrain topology.

The goal of kinematics modeling is to relate the motion of the rover body to the motions of the wheels, and vice versa. In order to achieve this, we attach a sequence of frames starting at the rover reference frame going to the suspension joints, steering, etc. and finally ending at the wheel–terrain contact frame. Let F_{i-1} and F_i be two consecutive frames in the sequence with their axes denoted by $(x_{i-1}, y_{i-1}, z_{i-1})$ and (x_i, y_i, z_i), respectively. Using the Denavit–Hartenberg (DH) parameters we can describe the transformation between these two frames. The four DH parameters are denoted here by $(\varepsilon_i, a_i, \lambda_i, d_i)$[1] where ε_i is the angle from z_{i-1} to z_i measured about x_{i-1}; a_i is the distance from z_{i-1} to z_i measured along x_i; λ_i is the angle from x_{i-1} to x_i measured about z_i and d_i is the distance from x_{i-1} to x_i measured along z_i. It is noted that the first two parameters (ε_i, a_i) are associated with the link between the two frames and are constant. On the other hand, either λ_i or d_i is variable, depending whether it is revolute or prismatic. The standard transformation from F_{i-1} to F_i is given by the matrix

$$T_{i-1,i} = \begin{bmatrix} c\lambda_i & -s\lambda_i & 0 & a_i \\ c\varepsilon_i s\lambda_i & c\varepsilon_i c\lambda_i & -s\varepsilon_i & -d_i s\varepsilon_i \\ s\varepsilon_i s\lambda_i & s\varepsilon_i c\lambda_i & c\varepsilon_i & d_i c\varepsilon_i \\ 0 & 0 & 0 & 1 \end{bmatrix} \tag{1}$$

where c and s denote cosine and sine functions respectively.

In the case of rovers, we are generally interested in the translational velocity vector $\dot{u}_i = [\dot{x}_i\ \dot{y}_i\ \dot{z}_i]^T$ and rotational velocity $\dot{\varphi}_i = [\dot{\alpha}_i\ \dot{\beta}_i \dot{\gamma}_i]^T$ vector, where α_i is the pitch, β_i is the roll and γ_i is the yaw. The 3×1 translational velocity vector $\dot{u}_i$ of the current frame F_i is dependent on the translational and rotational velocities of the previous frame F_{i-1}, plus translational velocity added to the frame F_i due to the motion of the current frame itself. The latter motion can be due to actuation. Using the conventional velocity propagation, the translation velocity can be written as [20]

$$\dot{u}_i = R_{i,i-1}\left(\dot{u}_{i-1} + \dot{\varphi}_{i-1} \times p_{i-1,i}\right) + \tilde{\dot{z}}_i \quad i = 1, 2, \ldots, n \tag{2}$$

where $R_{i,i-1}$ is the rotation matrix that rotates the axes of the frame F_{i-1} to coincides with those of the frame F_i; $p_{i-1,i}$ is the position vector of the origin of the coordinate frame F_i expressed in coordinate frame F_{i-1}; and $\tilde{\dot{z}}_i$ is the translational velocity added to the frame F_i due to the velocity of the frame F_i itself. The rotational velocity of the current frame F_i is [20]

$$\dot{\varphi}_i = R_{i,i-1}\dot{\varphi}_{i-1} + \tilde{\dot{\gamma}}_i \quad i = 1, 2, \ldots, n. \tag{3}$$

Eq. (3) indicates that the rotational velocity of the frame F_i is the sum of the effects of the rotational velocity of the frame F_{i-1} plus any rotational velocity $\tilde{\dot{\gamma}}$ added to the frame F_i. The latter is caused by the joint associated with frame F_i. Eqs. (2) and (3) are not in a form that can be used in a straightforward manner. Our goal is to develop a universal method to model the frame to frame motion starting from the rover reference frame and eventually reaching a wheel–terrain contact frame. This will be achieved through an extended and augmented DH table, to be described later.

[1] $(\varepsilon_i, a_i, \lambda_i, d_i)$ is equivalent to $(\alpha_{i-1}, a_{i-1}, \theta_i, d_i)$ in the conventional DH notation.

Using (1), we can extract the position vector $p_{i-1,i}$ to be used in (2) as

$$p_{i-1,i} = \begin{bmatrix} a_i \\ -d_i s\varepsilon_i \\ d_i c\varepsilon_i \end{bmatrix}. \tag{4}$$

The cross product in (2) can be written as

$$\dot{\varphi}_{i-1} \times p_{i-1,i} = \dot{\varphi}_{i-1} \times \begin{bmatrix} a_i \\ -d_i s\varepsilon_i \\ d_i c\varepsilon_i \end{bmatrix} = S_{i-1,i}\dot{\varphi}_{i-1} \tag{5}$$

where

$$S_{i-1,i} = \begin{bmatrix} 0 & d_i c\varepsilon_i & d_i s\varepsilon_i \\ -d_i c\varepsilon_i & 0 & a_i \\ -d_i s\varepsilon_i & -a_i & 0 \end{bmatrix} \tag{6}$$

and $S_{i-1,i}$ is a skew symmetric matrix. In order to obtain the rotation matrix $R_{i,i-1}$ needed in (2) and (3), we must find the transformation from frame i to $i-1$ which is the inverse of the homogeneous transformation matrix (1), i.e.

$$T_{i,i-1} = (T_{i-1,i})^{-1} = \begin{bmatrix} c\lambda_i & c\varepsilon_i s\lambda_i & s\varepsilon_i s\lambda_i & -a_i c\lambda_i \\ -s\lambda_i & c\varepsilon_i c\lambda_i & s\varepsilon_i c\lambda_i & a_i s\lambda_i \\ 0 & -s\varepsilon_i & c\varepsilon_i & -d_i \\ 0 & 0 & 0 & 1 \end{bmatrix}. \tag{7}$$

We extract the rotation matrix $R_{i,i-1}$ from (7) as

$$R_{i,i-1} = \begin{bmatrix} c\lambda_i & c\varepsilon_i s\lambda_i & s\varepsilon_i s\lambda_i \\ -s\lambda_i & c\varepsilon_i c\lambda_i & s\varepsilon_i c\lambda_i \\ 0 & -s\varepsilon_i & c\varepsilon_i \end{bmatrix}. \tag{8}$$

We must now find the translational and rotational velocities $\tilde{\dot{z}}_i$ and $\tilde{\dot{\gamma}}$ added to the frame i due to the motions of the same frame i, and to this end we must determine $\dot{T}_{i,i}$. Note that $T_{i,i}$ is an identity matrix but $\dot{T}_{i,i}$ is not a zero matrix. Taking the derivative of (1) and noting that ε_i and a_i are constant ($\dot{\varepsilon}_i = \dot{a}_i = 0$) since they are associated with links connecting two frames, we obtain

$$\dot{T}_{i-1,i} = \begin{bmatrix} (-s\lambda_i)\,\dot{\lambda}_i & (-c\lambda_i)\,\dot{\lambda}_i & 0 & 0 \\ (c\varepsilon_i c\lambda_i)\,\dot{\lambda}_i & (-c\varepsilon_i s\lambda_i)\,\dot{\lambda}_i & 0 & (-s\varepsilon_i)\,\dot{d}_i \\ (s\varepsilon_i c\lambda_i)\,\dot{\lambda}_i & (-s\varepsilon_i s\lambda_i)\,\dot{\lambda}_i & 0 & (c\varepsilon_i)\,\dot{d}_i \\ 0 & 0 & 0 & 0 \end{bmatrix}. \tag{9}$$

The derivative $\dot{T}_{i,i}$ is obtained from (9), by setting

$$\varepsilon_i = a_i = \lambda_i = d_i = 0 \tag{10}$$

which gives

$$\dot{T}_{i,i} = \begin{bmatrix} 0 & -\dot{\lambda}_i & 0 & 0 \\ \dot{\lambda}_i & 0 & 0 & 0 \\ 0 & 0 & 0 & \dot{d}_i \\ 0 & 0 & 0 & 0 \end{bmatrix}. \tag{11}$$

Finally, $\dot{T}_{i,i}$ can also be found, in terms of the translational and rotational velocities for a general body in motion, which is given by Craig [20]

$$\dot{T}_{i,i} = \begin{bmatrix} 0 & -\tilde{\dot{\gamma}}_i & -\tilde{\dot{\beta}}_i & -\tilde{\dot{x}}_i \\ -\tilde{\dot{\gamma}}_i & 0 & -\tilde{\dot{\alpha}}_i & -\tilde{\dot{y}}_i \\ -\tilde{\dot{\beta}}_i & -\tilde{\dot{\alpha}}_i & 0 & -\tilde{\dot{z}}_i \\ 0 & 0 & 0 & 0 \end{bmatrix}. \tag{12}$$

Comparing (11) and (12) we note that several components of (12) are zero for the case of the link/joint motion due to constraints. Equating the like terms in (11) and (12), we obtain $\tilde{\dot{x}}_i = \tilde{\dot{y}}_i = \tilde{\dot{\alpha}}_i = \tilde{\dot{\beta}}_i = 0$, $\tilde{\dot{z}}_i = \tilde{\dot{d}}_i$ and $\tilde{\dot{\gamma}}_i = \tilde{\dot{\lambda}}_i$. The reason for several elements of $\dot{T}_{i,i}$ being zero is that the link/joint in the kinematics chain has a constrained motion.

We now have all the terms needed in (2) and (3) in terms of the DH parameters and their derivatives. Substituting (5), (6) and (8) into (2)–(3), we obtain

$$\begin{bmatrix}\dot{u}_i\\ \dot{\varphi}_i\end{bmatrix} = \begin{bmatrix}R_{i,i-1} & R_{i,i-1}S_{i-1\cdot i}\\ 0 & R_{i,i-1}\end{bmatrix}\begin{bmatrix}\dot{u}_{i-1}\\ \dot{\varphi}_{i-1}\end{bmatrix} + \begin{bmatrix}b & 0\\ 0 & b\end{bmatrix}\begin{bmatrix}\dot{d}_i\\ \dot{\lambda}_i\end{bmatrix} \quad i = 1, 2, \ldots, n \tag{13}$$

where $S_{i-1,i}$ and $R_{i,i-1}$ are given by (6) and (8), respectively, $b = [0\ 0\ 1]^T$, $i = 0$ denotes the rover reference frame, $i = n-2$ is the wheel axle frame and the frames between these two frames are for various linkage and joints connecting the rover body to the wheel axle. The last two frames, i.e. $n-1$ and n, will be explained later.

Eq. (13) is a fundamental result that relates the motions of two consecutive frames in terms of certain rover parameters. These parameters are obtained from an extended and augmented DH table, referred to here as DHT table. In the DHT table, the first four columns are the same as those in DH table, i.e. (ε_i, a_i, λ_i, d_i), the next two columns consist of $\dot{\lambda}_i$ and $\dot{d}_i$ (see Table 1 to be explained later), and the joints are identified as either passive or active, and sensed or un-sensed. A non-zero $\dot{\lambda}_i$ or $\dot{d}_i$ indicates that the corresponding revolute or prismatic joint is variable. A variable joint can be either complaint (passive) or actuated (active). In an articulated rover a variable passive joint is used for compliance of the rover to the terrain. On the other hand an actuated (active) joint can be adjusted as desired. In our DHT table, we show the table entry for $\dot{\lambda}_i$ or $\dot{d}_i$ in bold face if it is compliant. Furthermore, any one of the four parameters (ε_i, a_i, λ_i, d_i) can be sensed/ known or un-sensed/unknown. Generally link lengths are known and joint angles are sensed. We show the unknown/un-sensed quantities in bold face in the DHT. As a result in addition to the four DH parameters, the DHT table identifies joints that are variable or fixed, joints that are passive or active and joints that are sensed or un-sensed. These identifications are needed for the derivation of rover kinematics modeling and for actuation to be discussed later.

The last frame in the chain, $i = n$, is the wheel–terrain contact where the motion over the terrain takes place. The contact frame F_n is shown in Fig. 1 where its x-axis, x_n, is tangent to the terrain at the point of contact and its z-axis, z_n, is normal to the terrain. In order to use the transformation from axle frame to contact frame using the DH table, we need to add one more intermediate frame, F_{n-1}, to the chain. Frames F_{n-1} and axle frame F_{n-2} share the same origin which is located at the center of the wheel. The wheel is assumed to be effectively represented by a rigid disk in contact with a non-deformable terrain. It is possible to derive wheel–terrain contact kinematics without these assumptions. However, the resulting kinematic model will become extremely complex and possibly not useful for analysis and control. The contact angle, denoted by δ, is the angle between the z-axis of the wheel axle z_{n-2} and the z-axis of the contact coordinate frame, as shown in Fig. 1. It is also the angle between x_{n-2} and x_{n-1}. The transformations from the wheel axle frame to the intermediate frame and then to the contact frame follow the same procedure as discussed before.

It is noted that the x components of translational velocity vector at the contact frame, is $\dot{x}_n = r\dot{\theta} + \dot{\xi}_n$ where $\dot{\theta}$ is the wheel angular velocity and $\dot{\xi}_n$ is the rolling slip. Similarly the y and z components of the translational velocity at the contact are, respectively, side slip $\dot{y}_n$ and bounce slip (up and down motion) $\dot{z}_n$. The rotational velocity components at the contact are tilt slip $\dot{\alpha}_n$, sway slip $\dot{\beta}_n$ and turn slip $\dot{\gamma}_n$. However, not all the six slips occur due to mechanical design and other physical constraints, otherwise the motions would become erratic and unpredictable.

Eq. (13) can be written in a more compact form as

$$\begin{bmatrix}\dot{u}_i\\ \dot{\varphi}_i\end{bmatrix} = \bar{P}_i\begin{bmatrix}\dot{u}_{i-1}\\ \dot{\varphi}_{i-1}\end{bmatrix} + B\begin{bmatrix}\dot{d}_i\\ \dot{\lambda}_i\end{bmatrix} \quad i = 1, 2, \ldots, n \tag{14}$$

Table 1
The DHT table for the multi-task rover.

Frame	ε_i	a_i	λ_i	d_i	$\dot{\lambda}_i$	$\dot{d}_i$
D	0	ℓ_1	0	ℓ_2	0	0
$SC14$	-90	0	$-90-\rho_1$	ℓ_3	$-\dot{\boldsymbol{\rho}}_1$	0
$SC23$	90	0	$90+\rho_2$	ℓ_3	$\dot{\boldsymbol{\rho}}_2$	0
$L1$	-90	ℓ_4	-90	ℓ_5	0	0
$L2$	90	ℓ_4	90	ℓ_5	0	0
$L3$	-90	ℓ_4	-90	ℓ_5	0	0
$L4$	90	ℓ_4	90	ℓ_5	0	0
$E1$	σ_1	0	0	d_0+d_1	0	$\dot{d}_1$
$E2$	$-\sigma_2$	0	0	d_0+d_2	0	$\dot{d}_2$
$E3$	σ_3	0	0	d_0+d_3	0	$\dot{d}_3$
$E4$	$-\sigma_4$	0	0	d_0+d_4	0	$\dot{d}_4$
$H1$	$-\sigma_1$	0	0	ℓ_6	0	0
$H2$	σ_2	0	0	ℓ_6	0	0
$H3$	$-\sigma_3$	0	0	ℓ_6	0	0
$H4$	σ_4	0	0	ℓ_6	0	0
$S1$	-90	0	ψ_1	$-\ell_7$	$\dot{\psi}_1$	0
$S2$	90	0	ψ_2	$-\ell_7$	$\dot{\psi}_2$	0
$S3$	-90	0	ψ_3	$-\ell_7$	$\dot{\psi}_3$	0
$S4$	90	0	ψ_4	$-\ell_7$	$\dot{\psi}_4$	0
$W1$	ρ_1	0	-90	0	0	0
$W2$	$-\rho_2$	0	90	0	0	0
$W3$	$-\rho_2$	0	90	0	0	0
$W4$	ρ_1	0	-90	0	0	0
$A1$	-90	0	$\boldsymbol{\delta}_1$	0	$\dot{\boldsymbol{\delta}}_1$	0
$A2$	90	0	$\boldsymbol{\delta}_2$	0	$\dot{\boldsymbol{\delta}}_2$	0
$A3$	90	0	$\boldsymbol{\delta}_3$	0	$\dot{\boldsymbol{\delta}}_3$	0
$A4$	-90	0	$\boldsymbol{\delta}_4$	0	$\dot{\boldsymbol{\delta}}_4$	0
$C1$	90	0	0	$-r$	0	0
$C2$	-90	0	0	$-r$	0	0
$C3$	-90	0	0	$-r$	0	0
$C4$	90	0	0	$-r$	0	0

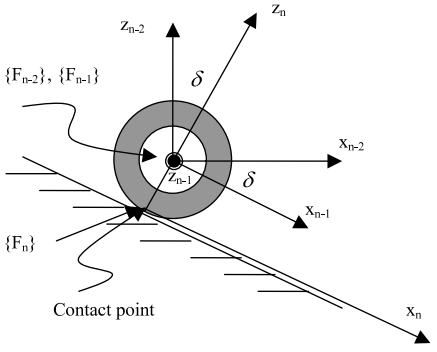

Fig. 1. Definition of contact angle.

where $\bar{P}_i$ and B are, respectively, 6×6 and 6×2 matrices given in (13). Observe that (13) describes the kinematics in a particular chain starting from the rover body frame and ending at one of the m wheels contact frame. In general the number of frames in each of the m chains can be different. Furthermore in general, contact angles at various wheels are different, i.e. we must use δ_j, $j = 1, 2, \ldots, m$. To take these aspects into consideration, it would be more precise to write (14) as

$$\begin{bmatrix}\dot{u}_{i_j}\\ \dot{\varphi}_{i_j}\end{bmatrix} = P_{i_j}\begin{bmatrix}\dot{u}_{i_{j-1}}\\ \dot{\varphi}_{i_{j-1}}\end{bmatrix} + B\begin{bmatrix}\dot{d}_{i_j}\\ \dot{\lambda}_{i_j}\end{bmatrix} \quad i = 1, \ldots, n,\ j = 1, 2, \ldots, m \tag{15}$$

where P_{i_j} and B are transformation matrices relating velocities of the frame $i-1$ to the frame i in the j-th chain, and there are n_j frames in this chain. It is noted that $\dot{d}_{i_j}$ is zero if the joint is revolute

and $\dot{\lambda}_{i_j}$ is zero if the joint is prismatic. Furthermore, if the joint is actuated, then either λ_{i_j} or d_{i_j} is adjustable otherwise the joint is compliant. Additionally, some joints/links may be common among several chains, as will be seen in the example of Section 4.

Contact kinematics describes the equation of the motion of a wheel at the contact frame $F_w \equiv F_n$ in terms of the motion of the rover reference frame $F_0 \equiv F_R$. This requires cascading the transformations in (15) to obtain an aggregate transformation for the kinematics chain. Since there are m wheels, there will be m such aggregate transformations which can be written as

$$\begin{bmatrix} \dot{u}_{wj} \\ \dot{\varphi}_{wj} \end{bmatrix} = P_{1_j} \begin{bmatrix} \dot{u}_R \\ \dot{\varphi}_R \end{bmatrix} + Q_j \dot{\eta}_j \quad j = 1, 2, \ldots, m \tag{16}$$

where $\dot{u}_{wj} \equiv \dot{u}_{(n_j)_j}$ and $\dot{\varphi}_{wj} \equiv \dot{\varphi}_{(n_j)_j}$ are the velocities at the j-th wheel–terrain contact; $j = 1, 2, \ldots, m$ and $\dot{u}_R \equiv \dot{u}_{(0_j)_j} \dot{\varphi}_R \equiv \dot{\varphi}_{(0_j)_j}$ are the velocities at the rover body frame, F_0, which are the same for all chains since all chains start at the rover body frame. The aggregate matrix $P_j = P_{0_j} P_{1_j} \cdots P_{(n-1)_j}$ is 6×6 and Q_j is a $6 \times 2n_j$ matrix similarly defined in terms of $Q_{0_j}, Q_{1_j}, \ldots, Q_{(n-1)_j}$ and $P_{0_j}, P_{1_j}, \ldots, P_{(n-1)_j}$. The $2n_j \times 1$ vector

$$\dot{\eta}_j = \left[(\dot{d}_{1_j} \dot{\lambda}_{1_j})^T \cdots (\dot{d}_{n_j} \dot{\lambda}_{n_j})^T \right]^T \quad j = 1, 2, \ldots, m \tag{17}$$

is the combined vector of parameter rates of all frames in the j-th chain.

The contact kinematics (16) can be used to determine the velocities at the wheel–terrain contacts for given rover reference frame velocities and the DHT parameter rates. Since $\dot{u}_j$ and $\dot{\varphi}_j$ contain various slip rates mentioned before, (16) can provide information about rover slippage behavior. This information, when processed, can be used in a control scheme for proper actuation. These aspects are beyond the scope of the present paper, and will not be discussed here.

We can also determine the velocities at the rover reference frame in terms of the wheel contact motions of various wheels. We will refer to this as *navigation kinematics* since it provides the position and orientation rates of the rover body. In the contact kinematics, we start from a single frame, i.e. rover reference frame, and branch off to several chains to reach different wheel contact frames. In the navigation kinematics, we do the reverse process. Thus the combined effects of motions at wheel–terrain contacts determine the rover body motion.

Using (13), the transformation in the reverse direction from the frame F_i to the frame F_{i-1} can be written as

$$\begin{bmatrix} \dot{u}_{i-1} \\ \dot{\varphi}_{i-1} \end{bmatrix} = \begin{bmatrix} R_{i,i-1} & R_{i,i-1} S_{i-1\cdot i} \\ 0 & R_{i,i-1} \end{bmatrix}^{-1} \left(\begin{bmatrix} \dot{u}_i \\ \dot{\varphi}_i \end{bmatrix} - B \begin{bmatrix} \dot{d}_{i_j} \\ \dot{\lambda}_{i_j} \end{bmatrix} \right) \quad i = n, \ldots, 1 \tag{18}$$

which simplifies to

$$\begin{bmatrix} \dot{u}_{i-1} \\ \dot{\varphi}_{i-1} \end{bmatrix} = \begin{bmatrix} R_{i,i-1}^T & S_{i-1,i} R_{i,i-1}^T \\ 0 & R_{i,i-1}^T \end{bmatrix} \begin{bmatrix} \dot{u}_i \\ \dot{\varphi}_i \end{bmatrix} + B_{i-1} \begin{bmatrix} \dot{d}_{i_j} \\ \dot{\lambda}_{i_j} \end{bmatrix} \quad i = n, \ldots, 1 \tag{19}$$

where $B_{i-1} = \begin{bmatrix} -R_{i,i-1}^T b & 0 \\ 0 & -R_{i,i-1}^T b \end{bmatrix}$. Note from (8) that $R_{i,i-1}^T = R_{i,i-1}^{-1} = R_{i-1,i}$.

Cascading transformations from wheel contact F_j to rover reference $F_0 \equiv F_R$, we can write (19) similarly to (16) as

$$\begin{bmatrix} \dot{u}_R \\ \dot{\varphi}_R \end{bmatrix} = G_j \begin{bmatrix} \dot{u}_j \\ \dot{\varphi}_j \end{bmatrix} + H_j \dot{\eta}_j \quad j = 1, 2, \ldots, m \tag{20}$$

where the subscript R denotes the rover reference, the matrices G_j and H_j are, respectively 6×6 and $6 \times 2n_j$ matrices obtained similarly to P_j and Q_j in (16). Eq. (20) describes the contributions of individual wheel motions to the rover body motion. The net body motion is the composite effect of motions of all wheels and can be obtained by writing (20) into a single matrix equation as

$$E \begin{bmatrix} \dot{u}_R \\ \dot{\varphi}_R \end{bmatrix} = G \begin{bmatrix} \dot{u}_w \\ \dot{\varphi}_w \end{bmatrix} + H \dot{\eta} \tag{21}$$

where $E = [I_6 \cdots I_6]^T$ is a $6m \times 6$ matrix, I_6 is the 6×6 identity matrix, $G = blockdiag\{G_j\}$ is the $6m \times 6m$ aggregate matrix, $\dot{u}_w = \left[\dot{u}_{C_1} T \quad \cdots \quad \dot{u}_{Cm}^T\right]^T$ and $\dot{\varphi}_w = \left[\dot{\varphi}_1^T \quad \cdots \quad \dot{\varphi}_m^T\right]^T$ are, respectively, $3m \times 1$ vectors of the aggregate translational and rotational velocities at the wheel contacts, $H = blockdiag\{H_j\}$ is the $6m \times \sum_{j=1}^{m} 2n_j$ matrix formed from H_j matrices, and $\dot{\eta} = \left[\dot{\eta}_1^T \quad \cdots \quad \dot{\eta}_m^T\right]^T$ is the $\sum_{j=1}^{m} 2n_j \times 1$ vector of aggregate DHT parameter rate vectors. Note that some elements of $\dot{\eta}$ are zero if their corresponding joint values/link lengths are fixed, in which case the dimensions of H and $\dot{\eta}$ are less than those just mentioned. There is little practical use for the *navigation kinematics* (21) on its own due to wheel slippage which results in odometry errors. However, (21) is very useful in deriving the actuation kinematics, to be discussed in the next section.

3. Rover actuation and balancing

Motion control of a rover requires determining commands to the actuators so that the rover body moves along a specified trajectory while achieving balanced rover configurations. The latter is required to avoid tip over when the rover traverses on a rough terrain. Actuators consist of wheel and steering motors as well as other motors (linear or rotational) that exist in an articulated high mobility rover.

We can partition the quantities in (21) into two sets; known and unknown. The known are measured (sensed) and specified quantities. Rovers are generally equipped with sensors such as accelerometers for measuring body pitch and roll angles, and joint values. The specified quantities are forward velocity of the rover body $\dot{x}_R$ and its yaw rate $\dot{\gamma}_R$. The specified quantities can also include some wheel slips such as tilt and sway slip rates; $\dot{\alpha}_j$ and $\dot{\beta}_j, j = 1, \ldots, m$; that are set to zero because of the mechanical construction that does not allow these motions. The unknown quantities consist of actuation quantities that need to be determined for the desired body motion, as well as quantities that are unmeasurable. The actuation quantities are the wheel roll rates $\dot{\theta}_j$, as well as articulated body actuators such as steering that constitute some components of $\dot{\eta}$ in (21). We partition the quantities in (21) into known (sensed or specified) identified by a bar superscript and unknown (to be found) identified by a tilde superscript as follows

$$\begin{bmatrix} \tilde{E} & \bar{E} \end{bmatrix} \begin{bmatrix} \tilde{\dot{u}}_R \\ \tilde{\dot{\varphi}}_R \\ \bar{\dot{u}}_R \\ \bar{\dot{\varphi}}_R \end{bmatrix} = \begin{bmatrix} \tilde{G} & \bar{G} \end{bmatrix} \begin{bmatrix} \tilde{\dot{u}}_w \\ \tilde{\dot{\varphi}}_w \\ \bar{\dot{u}}_w \\ \bar{\dot{\varphi}}_w \end{bmatrix} + \begin{bmatrix} \tilde{H} & \bar{H} \end{bmatrix} \begin{bmatrix} \tilde{\dot{\eta}} \\ \bar{\dot{\eta}} \end{bmatrix} \tag{22}$$

where $\tilde{E}$ and $\bar{E}$ are appropriate submatrices of E with dimensions of, respectively, $6m \times \tilde{n}$ and $6m \times (6 - \tilde{n})$ where $\tilde{n}$ is the number of unknown rover position and orientation components. The submatrices $\tilde{G}$, $\bar{G}$, $\tilde{H}$ and $\bar{H}$ are similarly defined. It is noted that actuation quantities are the components of $\bar{\eta}$. Eq. (22) is rearranged by forming a vector consisting of all unknown quantities on one side of the equation and the unknown quantities on the other side

to obtain

$$\begin{bmatrix}\tilde{E} & -\tilde{G} & -\tilde{H}\end{bmatrix}\begin{bmatrix}\dot{\tilde{u}}_R\\ \dot{\tilde{\varphi}}_R\\ \dot{\tilde{u}}_w\\ \dot{\tilde{\varphi}}_w\\ \dot{\tilde{\eta}}\end{bmatrix}=\begin{bmatrix}-\bar{E} & \bar{G} & \bar{H}\end{bmatrix}\begin{bmatrix}\dot{\bar{u}}_R\\ \dot{\bar{\varphi}}_R\\ \dot{\bar{u}}_w\\ \dot{\bar{\varphi}}_w\\ \dot{\bar{\eta}}\end{bmatrix}. \tag{23}$$

Eq. (23) can be written in the more compact form of

$$A\dot{\tilde{X}}=B\dot{\bar{X}} \tag{24}$$

where $A=[\tilde{E}-\tilde{G}\,\tilde{H}]$, $B=[-\bar{E}\,\bar{G}\,\bar{H}]$, and $\dot{\tilde{X}}$ and $\dot{\bar{X}}$ are vectors of unknown and known quantities defined in (23).

Eq. (24) is in the standard form and can be solved for the unknown vector $\dot{\tilde{X}}$, when a solution exists. The condition for the existence and uniqueness of the solution are well known for the given A and B (e.g. see [13]). The solution to (24) gives $\dot{\tilde{X}}$ from which the actuation quantities $\tilde{\eta}$, as well as navigation quantities of interest, e.g. rover position rates $(\dot{x}_R, \dot{y}_R)$ and heading rate $\dot{\gamma}_R$ can be extracted. Other components of $\dot{\tilde{X}}$ are obtained as by a product.

In general high mobility rovers have more unknown than known quantities and the system of Eqs. (24) is underdetermined. This implies that additional requirements can be included to take advantage of the extra degrees of freedom offered by (24). The freedom is brought about due to extra actuators in an active suspension system. We will use the extra freedom to balance the rover configuration as it moves over rough terrain. In such terrain with many bumps and dips, without balance control, the rover can loose balance and can tip over. We must now define and quantify more precisely the notion of a balanced configuration and express it in terms of rover orientation angles and adjustable joint angles. Stability measures have been suggested before, e.g. [17]. Here, we use wheel–terrain contact position vectors u_j, which represent vectors drawn from the rover reference point to the wheel–terrain contact point. Each consecutive pair of vectors (i.e., u_j and u_{j+1}) form a plane denoted by π_j. The unit vector perpendicular to this plane is given by

$$\bar{s}_j=\frac{u_j\times u_{j+1}}{\|u_j\times u_{j+1}\|}\quad j=1,\ldots,m;\ u_{m+1}=u_1. \tag{25}$$

Suppose that the rover reference frame R is at the center of rover mass, the rover unit gravity vector $\bar{g}$ can be expressed in terms of sines and cosines of pitch and roll angles as

$$\bar{g}=\begin{pmatrix}s(\beta_R) & -s(\alpha_R)\,c(\beta_R) & -c(\alpha_R)\,c(\beta_R)\end{pmatrix}^T. \tag{26}$$

Now consider the dot product between unit vectors s_j and $\bar{g}$, i.e.

$$\mu_j=\bar{g}^T\,\bar{s}_j. \tag{27}$$

When the gravity vector $\bar{g}$ lies in any of the planes π_j, the vectors $\bar{g}$ and s_j become orthogonal, resulting in $\mu_j=0$ and the rover comes to the verge of tipping over. On the other hand, when the vectors $\bar{g}$ and s_j are along the same direction, $\mu_j=1$ for all planes, and the rover is in the most stable configuration. We define the tip over measure as the aggregate of all μ_j, i.e. $\mu=-\prod_{j=1}^{m}\mu_j$. Higher values of μ corresponds to a higher possibility of tip over.

Now we define a *balanced rover configuration* as one that has a low tip over measure μ, has body pitch α_R and body roll β_R close to zero, and is close to its nominal configuration. The latter is a configuration that the rover attains when moving on a flat surface. We must now formulate an objective function whose optimization results in a balanced configuration. Consider minimization of an objective function of the form

$$f=a_1\,\mu+a_2\,(\alpha_R^2)_{nrm}+a_3\,(\beta_R^2)_{nrm}+a_4\,\|\tilde{\eta}_a-\tilde{\eta}_{an}\|_{nrm} \tag{28}$$

where the subscript *nrm* denotes the normalized value, which is obtained by dividing the value by its maximum. Therefore, the normalized range of last three terms in (28) is 0–1. The first term μ is the tip over measure, and it range is -1 and 0 and which is already normalized. The normalized pitch and roll, i.e. second and third terms in (28), must be minimized to keep the rover body level. The vector $\tilde{\eta}_a$ represents the actuated suspension joints which is a sub-vector of the unknown $\tilde{\eta}$, and $\tilde{\eta}_{an}$ is the nominal value of $\tilde{\eta}_a$ which is the value when the rover moves on a flat surface. Note that without the fourth term, minimizing f would result in a rover configuration that is maximally flat, that is legs spread out even when the rover moves over a flat surface. The maximum value of $\|\tilde{\eta}_a-\tilde{\eta}_{an}\|$ needed for normalization dependent on the particular rover. The weighting factors a_1, a_2, a_3 and a_4 place relative emphasis between achieving rover balancing and the desire to operate near the nominal configuration.

The balance and motion control problem may be stated as follows. Given the desired rover forward speed $\dot{x}_d$ and heading γ_d, determine the commands to the wheel and actuated joints, which include the steering, such that the rover maintains the desired forward speed and heading while minimizing the criterion (28). In other words, it is required to minimize (28) subject to (24). The solution to such constrained optimization is [21].

$$\tilde{X}=A^{\#}B\bar{X}-k(E-A^{\#}A)\begin{pmatrix}\partial f/\partial\tilde{\eta}_a\\ 0\end{pmatrix} \tag{29}$$

where $A^{\#}$ is the pseudo-inverse of A, k is a scalar, E is an identity matrix, $\partial f/\partial\tilde{\eta}_a$ is the vector of the gradient of the performance function with respect to the actuated suspension joints, and the zero vector is of appropriate dimension to make the dimensions compatible. The gradient is computed numerically. The unknown vector $\tilde{X}$ consists of the actuated values, rover position and heading and other unknown which such as rolling slip or sides slip. The actuated vector provides the set-points for various motors. Standard controllers, i.e. PID controllers, can then be employed to achieve these set points. Such controllers can be placed on an outer loop and act on the error between the desired rover motion, i.e. forward velocity $\dot{x}_d$ and yaw rate $\dot{\gamma}_d$ and their actual values to keep the rover on the desired trajectory. However, the focus of this paper is rover kinematics analysis, actuation and balancing. As such, dynamics stability analysis and trajectory tracking are not investigated in this paper.

It is to be noted that trajectory tracking and optimization of a performance index such as (28) may be in competition and conflict if the rover does not have sufficient degrees of freedom and moves over ragged terrain. In such cases, tasks prioritization can be employed [21], e.g. by assigning a higher priority to balancing when the rover is near the tip over situation. For high mobility rovers, such as the one to be described in Section 4, both balancing and tracking can be generally achieved.

We have developed a Matlab program to determine various kinematics forms of a general articulated rover. The input to the program is the rover DHT table. As mentioned before, this table contains in addition to the four DH parameter columns, two columns for the joint rates $\dot{\lambda}_i$ and $\dot{d}_i$ which can be passive (compliant) or active (actuated). Generally both active and passive quantities are sensed. The separation of active and passive components is needed for computing actuation kinematics. When an element of $\dot{\eta}_j$ in (16) is zero, the corresponding column of the matrix of Q_j is removed. Using the DHT table, the aforementioned program solves (16), (21) or (24) and provides contact, actuation or navigation kinematics in either symbolic or numeric form, as desired.

We have also developed a simulation environment for computing and showing the motion of high mobility rovers over any desired terrain. It consists of several modules as shown in Fig. 2. The

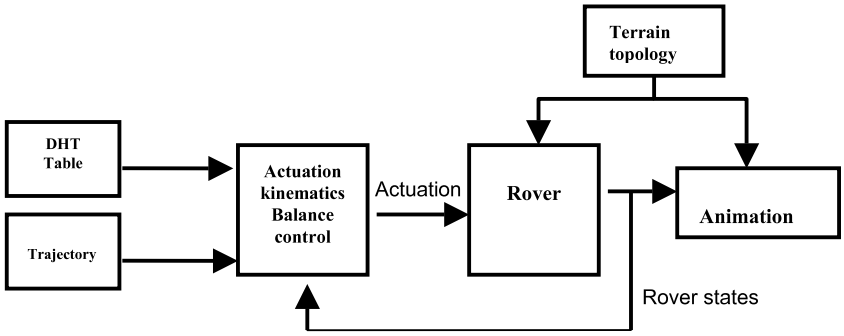

Fig. 2. Rover actuation and balance control block diagram.

DHT table contains the information about the motion kinematics of the rover as described before. The trajectory specifies the desired velocity and turning rate of the rover as a function of time. The actuation and balance control module uses the received the DHT table, the desired trajectory and the current sensed rover quantities such as rover body roll, pitch and yaw angles, as well as passive and active joint angles, steering angles, etc. This module and produces actuation signals via (29) which are used by the rover.

The terrain is generated by a mathematical function $z = f(x, y)$ specifying the elevation at each point on the terrain. This function can also be generated using a natural terrain image, as in the terrain used in Section 4. The rover receives the actuation signals and terrain topology. It then applies the incremental actuation values such as steering, leg actuation and wheel rolling to the rover. The new wheel contact positions and orientations are computed by the rover module. Since the rover wheels must be in contact with the terrain, this module also determines the passive joint angles to ensure proper wheel–terrain contact [13]. If one or more wheels cannot be contacted with the terrain, the computations are performed using the contacting wheels. After the incremental move and adjustments for the rover to conform to the terrain, the sensed values are sent to the actuation kinematics and balance control for determining the next set of actuations. It is to be noted that a control loop can be added for trajectory tracking, if it is desired. In this case a controller receives the desired rover trajectory and compares it with actual trajectory from the rover.

We have applied the above procedure to several rovers including NASA's Rocky 7 and Sample Return rovers and the multi-tasking rover, MTR. The latter will be discussed below.

4. Example—multi-task rover

The rover to be considered here is highly articulated and is called multi-task rover (MTR), [22]. It is shown in Fig. 3, and integrates mobility, modularity and re-configurability. Instead of attaching to MTR specific tools or instruments, its main chassis is reconfigurable in such a way that it can mechanically couple with packs, such as science packs or tool packs. Each pack is a robotic mechanism which works independently, and serves for a particular purpose. For instance, it can be a manipulator with gripper end-effector to collect rock and soil samples. The mobility of MTR is the main interest of this paper. We first introduce its basic structure and characteristics, then develop the DHT table and for deriving the kinematics model. A video [23] demonstrates the mobility of the system and aids in following the description below.

4.1. Structure of the multi-task rover

The MTR has four legs in which each leg is attached to a wheel and has three degrees of freedom. In each leg, there is one motor for wheel rolling; one motor for steering and a linear actuator that changes the geometry of the leg (see Fig. 4). The rover main body has an active differential with two degrees of freedom in which two motors are linked to a body shaft via two spring loaded pulley drives, as shown in Fig. 4. There are, therefore, a total of fourteen motorized actuators, twelve for the legs and two for the body to ensure proper operation of three subsystems: steering/drive subsystem, shoulder articulation subsystem, and active differential subsystem.

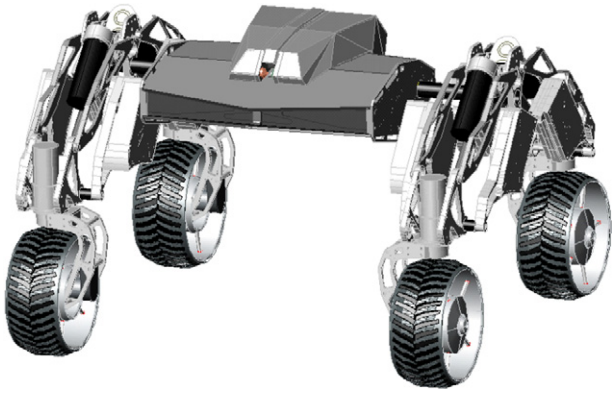

Fig. 3. Multi-tasking rover.

Steering-drive subsystem is responsible for steering and rotational velocity of the wheels. Each wheel is independently steered, however, the two steering axes of each side of the rover are kept in parallel by mechanical design.

Shoulder articulated subsystem is used to adjust the angle between two legs connected to a shoulder on one side. The linear actuator in each leg plays an important role and acts like an adjustable diagonal in a parallelogram consisting of four bars. The vertices are hinges and as the diagonal change its length by the linear actuator, the geometry of the leg changes. Fig. 5 shows examples of leg configurations on one side of the rover when the diagonal length changes. By combining the changes of all four legs, the MTR can achieve some interesting geometrical configurations such as:

- Moving the body up/down by lifting/lowering all legs.
- Leaning the body forward by lowering the front leg and extending the rear leg, (and vice versa for leaning backward).
- Altering the rover roll angle by lifting one shoulder while lowering the other.
- Rotating the rover about its yaw axis by giving equal and opposite deflection to certain leg pairs.

The active differential system has two DC motors and serves two purposes:

- Adjusting the angle between a shoulder and the body.
- Allowing the body to rotate around its pivot point to the shoulder. One condition for this to happen is that both motors

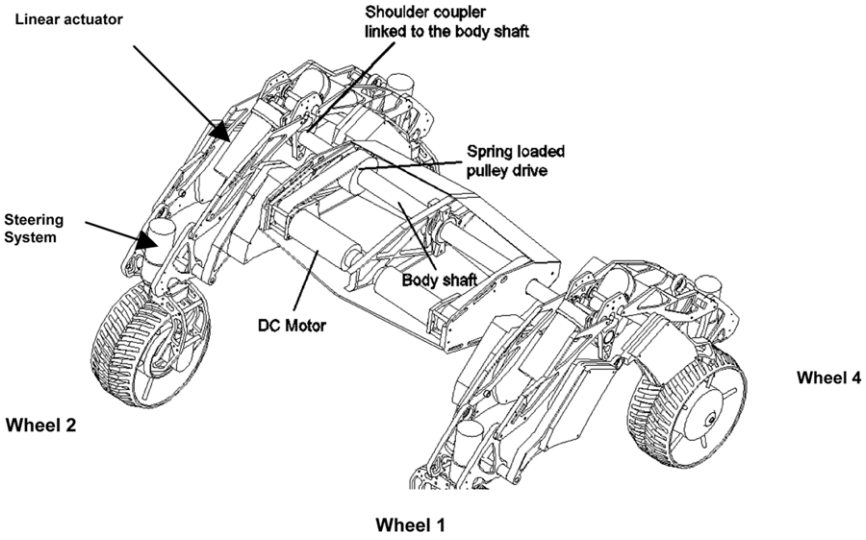

Fig. 4. Components of the multi-task rover.

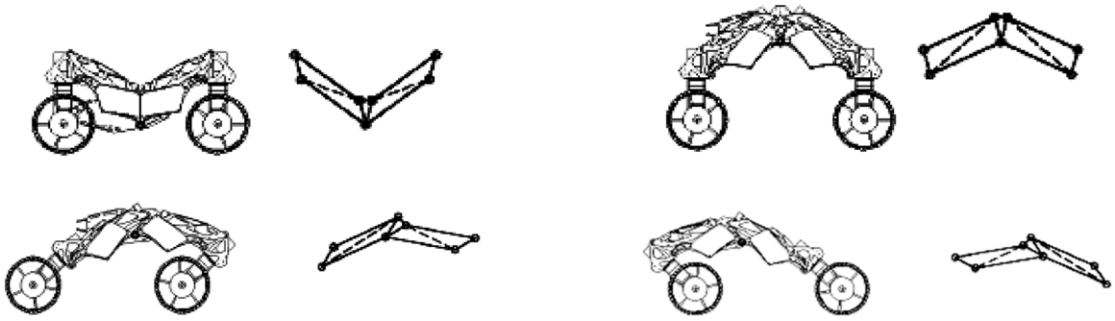

Fig. 5. Examples of rover configurations achieved through legs linear actuators.

have to rotate in the same direction. This feature is also used to reallocate the center of mass and flip the main body by 180° so that it can pick up and hold objects.

Each body shaft is linked to a DC motor–gearbox combination via a synchronous pulley drive that provides for the adjustment of rotation. Each pulley drive is allowed a ±5° spring-loaded backlash, so it gives a passive compliance to the active differential system. It is designed to effectively sense if all wheels are in contact with the ground during traversal over rough terrain. As a result, the wheels can be forced to touch the ground passively by the rover weight.

4.2. The DHT table

In this section, we assign coordinate frames and set up the DHT table. The diagram in Fig. 6 shows the reference frame $\{R\}$ located at the center of the mass, differential frame $\{D\}$ placed at the middle of body shaft connecting the two shoulder couplers. The horizontal and vertical distances from the origin of $\{R\}$ to the origin of $\{D\}$ are denoted, respectively, by ℓ_1 and ℓ_2. The row of the DHT table for the differential frame $\{D\}$ is as shown in Table 1. Note that since the origins of $\{R\}$ and $\{D\}$ are the same, $\ell_1 = \ell_2 = 0$. Furthermore, because of the constant values of $\dot{\lambda}_i$ and $\dot{d}_i$, the last two columns for the frame $\{D\}$ are zero.

The shoulder coupler frames $\{SC14\}$ and $\{SC23\}$ are located at either end of the body shaft with z-axis pointing out and x-axis pointing up with rotation angles ρ_1 and ρ_2 about the body shaft. These angles provide passive compliance of the rover with the terrain. The half width of the rover which is the distance between the origins of the frames $\{D\}$ and either shoulder coupler is denoted by ℓ_3, which for the MTR is $\ell_3 = 274$ mm. With assigned axes, angles and lengths; the rows corresponding to $SC14$ and $SC23$ are as indicated in Table 1. Note that the angles ρ_1 and ρ_2 are variable but unactuated, therefore the values of $\dot{\lambda}_i$ are as shown in the table for the frames $\{SC14\}$ and $\{SC23\}$, whereas $\dot{d}_i$ is zero due to the constant length ℓ_3.

The shoulder coupler frame $\{SC14\}$ on the right side leads to the front wheel $W1$ and the back wheel $W4$. Similarly the left shoulder coupler $\{SC23\}$ branches off to the left front and left back wheels $W2$ and $W3$, respectively. Fig. 7 shows the kinematic arrangement of the right side of the rover including frames assignments. The frames for the right front leg are coupler $\{SC14\}$, leg 1 $\{L1\}$, end of linear actuator $\{E1\}$, heap $\{H1\}$, steering $\{S1\}$ and wheel $\{W1\}$. The steering angle and the wheel roll angle are denoted by ψ_1 and θ_1, respectively. Similar frames are assigned for the right back leg with the frame $\{L4\}$.

The leg frame $\{L1\}$ is considered next with the aid of Fig. 7. The leg frame $\{L1\}$ is reached from the shoulder coupler frame $\{SC14\}$ by constants $\ell_4 = 35.9$ mm and $\ell_5 = 17$ mm. The length ℓ_4 is the distance between the origin of $\{SC14\}$ and the middle point of the line connecting the origins of $\{L1\}$ and $\{L4\}$, and the length ℓ_5 is half the distance between origin of $\{L1\}$ and $\{L4\}$. The x-axis of $\{SC14\}$ is always perpendicular to line connecting the origins of $\{L1\}$ and $\{L4\}$. The other leg frames are treated similarly. Thus we have the rows of DHT table for $\{L1\}$ through $\{L4\}$, as shown in Table 1.

The adaptability and re-configurability of this rover bring some complexity to its kinematics modeling. Unlike most other rovers where legs are rigid, in this rover the linear actuator modifies the geometry of each leg. When this actuator is extracted or retracted,

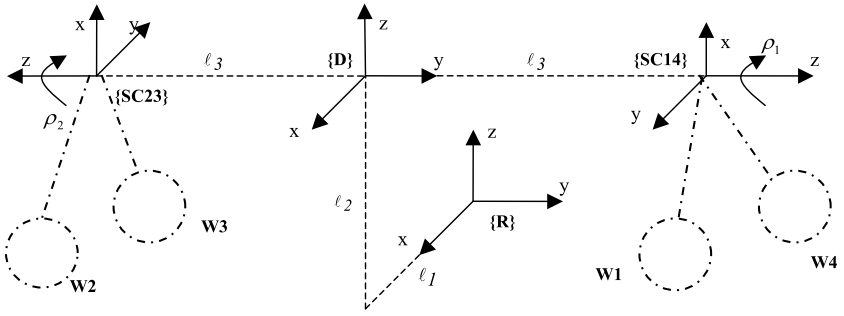

Fig. 6. Frame assignments for the rover reference, differential and shoulder couplings.

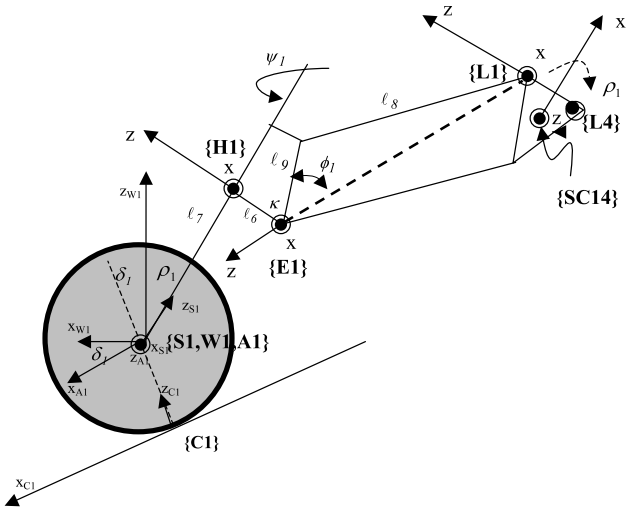

Fig. 7. Assignment of frames from right shoulder coupler to right front wheel.

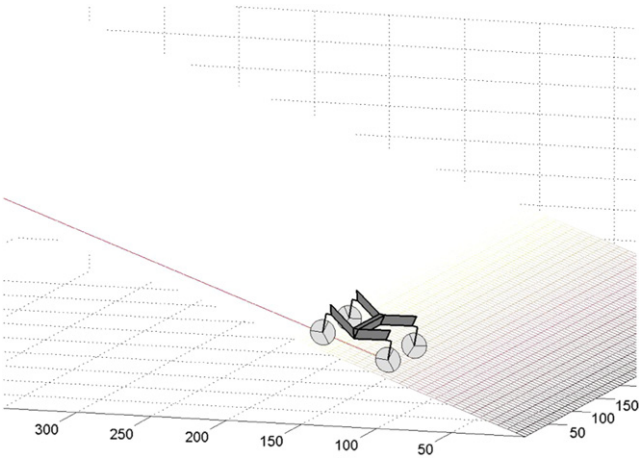

Fig. 8. Rover moving down a 20° slope.

the shape of the leg changes and its side-effect creates some rotation angles among frames. Referring to Fig. 7, the diagonal length shown a by the dotted line, is adjusted by the linear actuator. Using this figure, we observe that to transform from the leg frame $\{Lk\}$ to the linear actuator frame $\{Ek\}$, $k = 1, 2, 3, 4$ we must rotate the z-axis of leg frame by σ_k to align it with the z-axis of the linear actuator frame where

$$\sigma_k = 180 - \tau - \phi_k \quad k = 1, 2, 3, 4 \tag{30}$$

where $\tau = 75.93°$ is computed based on the linkage lengths, and the angle ϕ_k is obtained using the laws of cosine as

$$\phi_k = a\cos\left(\frac{\ell_9^2 + (d_0 + d_k)^2 - \ell_8^2}{2\ell_9(d_0 + d_k)}\right) \quad k = 1, 2, 3, 4 \tag{31}$$

where $\ell_8 = 213$ mm $\ell_9 = 70$ mm are the lengths of the sides of the parallelogram, as shown in Fig. 7; $(d_0 + d_k)$ is the length of the diagonal shown as dotted line, $d_0 = 165.5$ mm is a constant joint offset of linear actuator (prismatic joint) which is the same for each leg, and d_k is the length of actually extended part of leg k, $k = 1, 2, 3, 4$. These lead to the rows for the frames $\{E1\}$ through $\{E4\}$ of the DHT table.

The transformation from $\{Ek\}$ to the hip frame $\{Hk\}$ requires a rotation σ_k in the opposite direction to that of $\{Lk\}$ to $\{Ek\}$ since the z-axis of $\{Hk\}$ is aligned with the z-axis of $\{Lk\}$, as seen from Fig. 7. To reach $\{Hk\}$ also requires a translation $\ell_6 = 35$ mm, as shown in Fig. 7. These justify the rows of DHT for the frames $\{Hk\}$, $k = 1, 2, 3, 4$. It is noted that since the lengths d_k are variable and actuated, therefore $\dot{d}_k$ appear in the corresponding column of $\{Hk\}$.

The next frame in the chain is steering frame $\{Sk\}$, reached from $\{Hk\}$ by distance $\ell_7 = 126$ mm, in which its z-axis is always parallel with x-axis of shoulder couple frame $\{SC14\}$, or $\{SC23\}$. The last three frames are wheel $\{Wk\}$, axle $\{Ak\}$, and contact $\{Ck\}$, where the first two share the same origin as the with the steering frame, as shown in Fig. 7. The relative rotations of these frames are shown in Fig. 7 where the contact angles of wheel to terrain δ_k are shown. As seen from Table 1, the contact angles and their rates are shown in bold face meaning that they are treated as un-sensed and un-actuated. These angles form part of the unknown vector $\tilde{\dot{X}}$ in (24) which are found by solving (24), as discussed before. Finally, the contact frame is as shown and is displaced from the axle frame by the wheel radius r. This completes the construction of the DHT table. The slippages are assumed to be zero to avoid mixing of different effects and complicating the results. Adding various slips would also make the table unnecessarily long.

The equation of motion from frame to frame can be set up using (6), (8), (13) and the DHT table. For example, we substitute the entries of second row of the DHT table into (6), (8) and (13) to express the motion of the right shoulder in terms of the motion of the differential frame as

$$\begin{bmatrix} \dot{u}_{sc14} \\ \dot{\varphi}_{sc14} \end{bmatrix} = \begin{bmatrix} -s\rho_1 & 0 & c\rho_1 & -\ell_3 c\rho_1 & 0 & \ell_3 s\rho_1 \\ c\rho_1 & 0 & s\rho_1 & \ell_3 s\rho_1 & 0 & -\ell_3 c\rho_1 \\ 0 & 1 & 0 & 0 & 0 & 0 \\ 0 & 0 & 0 & -s\rho_1 & 0 & c\rho_1 \\ 0 & 0 & 0 & c\rho_1 & 0 & s\rho_1 \\ 0 & 0 & 0 & 0 & 1 & 0 \end{bmatrix} \times \begin{bmatrix} \dot{u}_D \\ \dot{\varphi}_D \end{bmatrix} + \begin{bmatrix} 0 \\ 0 \\ 0 \\ 0 \\ 0 \\ 1 \end{bmatrix} \dot{\rho}_1. \tag{32}$$

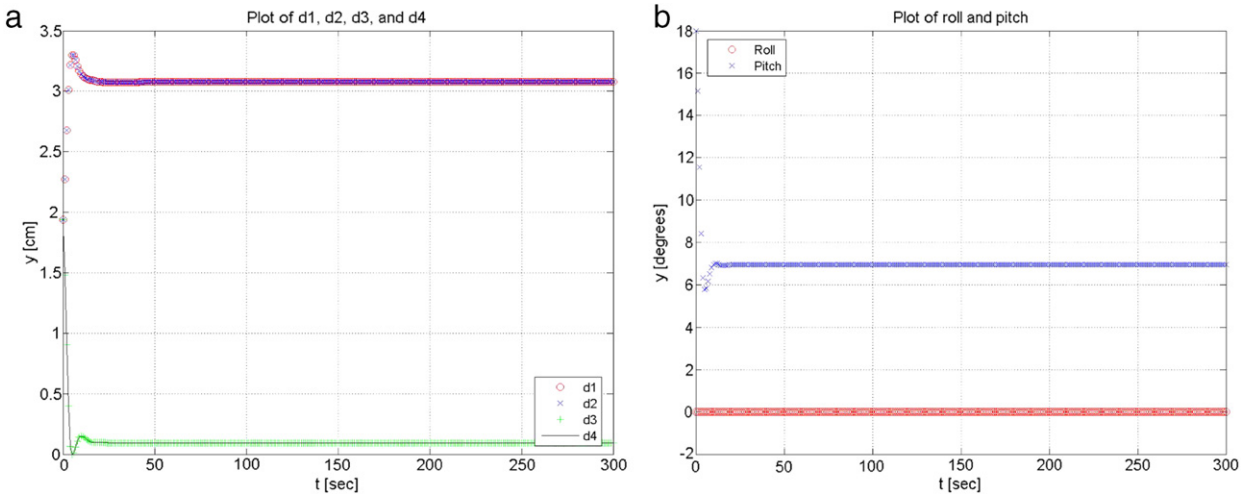

Fig. 9. (a) Actuator leg lengths and (b) rover body pitch and roll for the inclined surface.

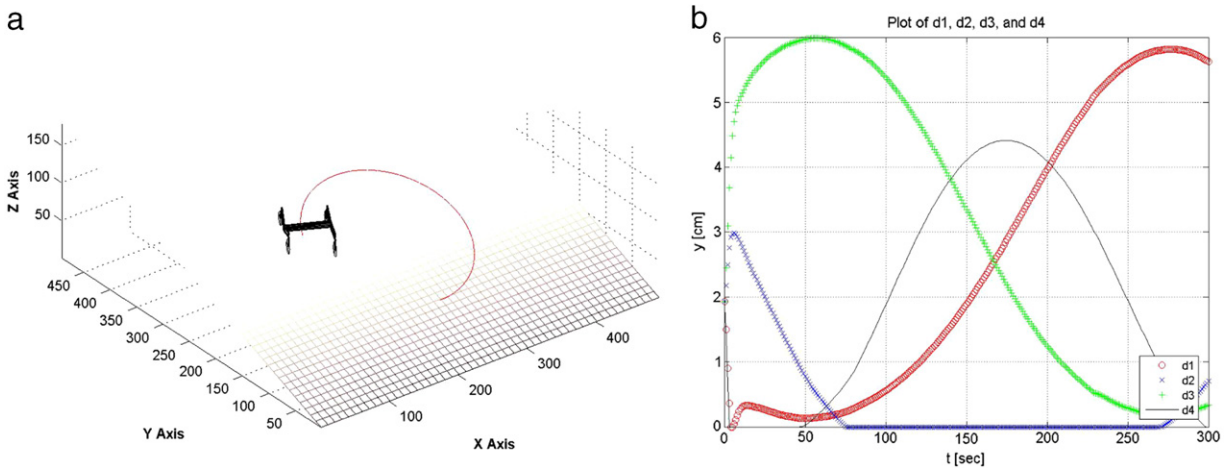

Fig. 10. (a) Rover moving on an inclined circular path, and (b) variations of the actuator lengths.

Note that the rotation rate about the body shaft $\dot{\rho}_1$ affects the yaw rate of the shoulder coupler. Similarly, using (6), (8) and (13), the motion of the linear actuator frame is expressed in terms of the motion of the leg frame as

$$\begin{bmatrix} \dot{u}_{E1} \\ \dot{\varphi}_{E1} \end{bmatrix} = \begin{bmatrix} 1 & 0 & 0 & 0 & -D_1 s\mu_1 & D_1 s\mu_1 \\ 0 & -s\mu_1 & c\mu_1 & -D_1 & 0 & 0 \\ 0 & -c\mu_1 & -s\mu_1 & 0 & 0 & 0 \\ 0 & 0 & 0 & 1 & 0 & 0 \\ 0 & 0 & 0 & 0 & -s\mu_1 & c\mu_1 \\ 0 & 0 & 0 & 0 & -c\mu_1 & -s\mu_1 \end{bmatrix} \times \begin{bmatrix} \dot{u}_{L1} \\ \dot{\varphi}_{L1} \end{bmatrix} + \begin{bmatrix} 0 \\ 0 \\ 1 \\ 0 \\ 0 \\ 0 \end{bmatrix} \dot{d}_1. \tag{33}$$

where $\mu_1 = 0.078\pi + \phi_1$, $D_1 = d_0 + d_1$ and ϕ_1 is given by (31). The motions of the other frames can be written similarly.

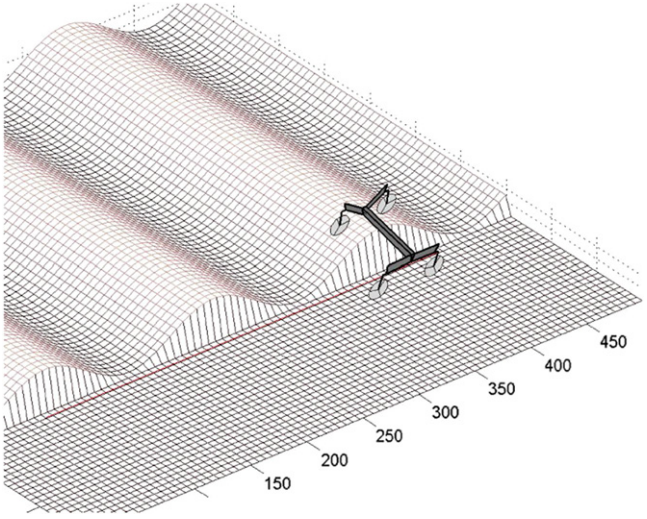

Fig. 11. Asymmetrical wavy terrain.

4.3. Results

In this section we discuss the results of applying the actuation kinematics and balancing to the MTR in several scenarios from simple to complex. In all experiments the rover actuator lengths are initially set at their nominal values which are $\tilde{\eta}_{an} = (d_1\ d_2\ d_3\ d_4)^T$ where $d_1 = d_2 = d_3 = d_4 = 1.938$ cm. The

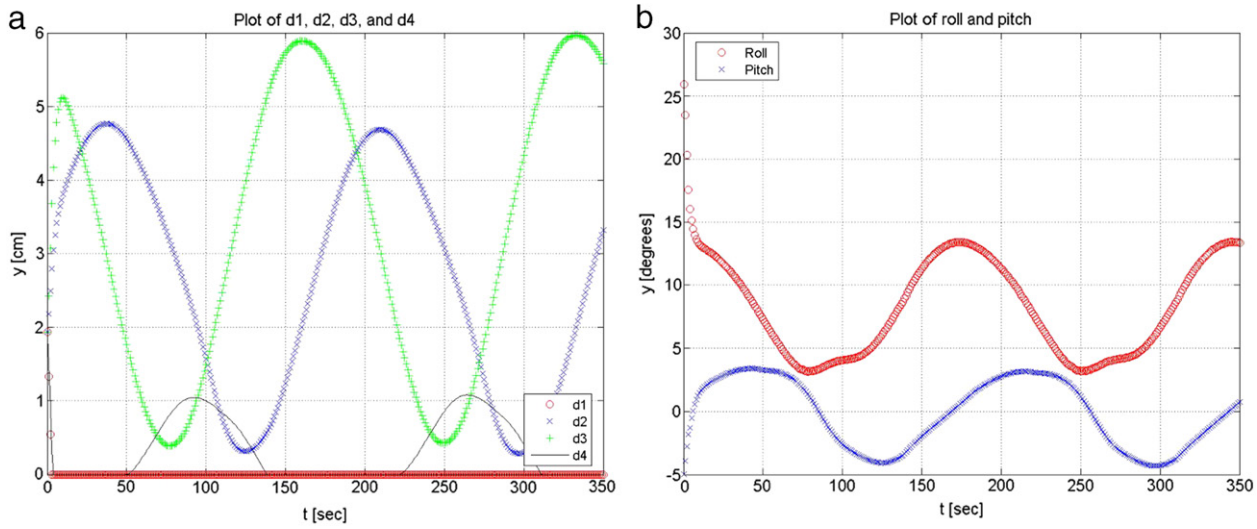

Fig. 12. (a) Actuator leg lengths and (b) rover body pitch and roll for wavy terrain.

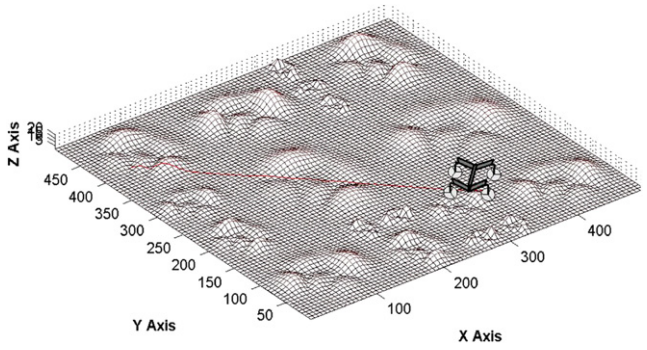

Fig. 13. A relatively complex terrain with bumps and ditches.

nominal values correspond to the rover placed on a flat surface. The maximum value of $\|\tilde{\eta}_a - \tilde{\eta}_{an}\|$ in (28) is estimated to be 8, and the maximum value of pitch and roll is each $\frac{\pi}{4}$ rad $= 45°$. In all experiments below the coefficients of the normalized optimization function (28) are $a_1 = 0.7, a_2 = a_3 = 2.56, a_4 = 2.4$. The latter indicates that for the experiments to be described, the pitch, roll and deviations from nominal configuration are weighted approximately the same, and less emphasis is placed on the tip over index. The dynamics of the leg actuators are not considered in the simulations since the time constant of actuators is low, i.e. they act fast compared to the relatively slow motion of the rover over rough terrain. Furthermore wheel slips that occur in rough environments have not been accounted for in the simulations, but are currently under investigation. It must be emphasized that in the following case studies the emphasis is on verifying rover kinematic modeling and its behavior as well as actuation and balancing rather than path trajectory tracking, since no closed loop control is employed in these experiments.

Case 1. *Inclined surface.*

The terrain is an inclined smooth surface with a slope of 20°, as shown in Fig. 8. The rover starts at $(x, y) = (40, 400)$ cm and moves downward along a straight line parallel to the y axis to the final location at $(x, y) = (40, 0)$. The 400 cm distance is traveled in 300 s.

The actuator lengths are shown in Fig. 9(a), and it is seen that the front leg length d_1 and d_2 quickly increase from the initial $d_1 = d_2 = 1.938$ cm to $d_1 = d_2 \approx 3.1$ cm whereas those of the back legs decrease from $d_3 = d_3 = 1.938$ to $d_3 = d_4 = 0$. This implies that the front legs are extended and while the back legs are retracted and the rover leans backward to keep the rover relatively flat resulting a balanced configuration. The rover body pitch and roll are plotted in Fig. 9(b), which shows that the pitch is reduced quickly from the 20° initial slope to about 7°. On the other hand, the roll is kept at zero throughout the motion since both sides (left and right) of the rover are at the same height. The rover pitch can be reduced further by increasing the coefficient a_2 in (28). It is also found that the rover follows the desired trajectory and the maximum error is about 3 cm. The tracking is achieved through the actuation kinematics without closed loop control. Adding an outer loop control will reduce the error to a small value.

We have also conducted an experiment moving the rover along x-axis (across the slope) starting from $(x, y) = (50, 150)$ cm and ending at $(x, y) = (450, 150)$ cm. The plots are not shown to save space. The actuator lengths now became $d_2 = 3.7$, $d_3 = 4.6$, and $d_1 = d_4 = 0$ which indicates that the legs on the right side are lifted and the legs on the left side are lowered, as it should be. The pitch and roll were small. The reason for d_2 and d_3 not being equal, and the non-zero pitch and roll is the interplay between various requirements in the criterion (28).

Case 2. *Circular path.*

Consider now the case where the rover moves on the inclined surface on a circular path as shown in Fig. 10(a). The time trajectories are given by $x = r \cos t + a$ and $y = r \sin t + b$ where r is the radius and a and b are the coordinates of the center of the circle. The actuator lengths as functions of time are shown in Fig. 10(b). It is noted that the leg lengths change in such a way to balance the rover. The sinusoidal type variations of the actuator lengths are due to the underlying sinusoidal time trajectories of the circular path. The pitch and roll (not shown due to space limitations) also undergo sinusoidal variations between $-7°$ and $+7°$ which are acceptable for a balanced operation. The maximum error between the actual and desired paths is 4.2 cm, which can be reduced by adding an outer loop controller, as discussed before.

Case 3. *Wavy terrain.*

In this case one side of the rover moves on a wavy terrain and the other side moves on a flat surface, as shown is Fig. 11. The equation of the elevation is given by $z(x, y) = h \sin(\frac{2\pi}{p}(x - a))$ where h, a and p determine the height, width and period of the bumps, respectively. The rover starts at $(x, y) = (50, 150)$ cm and moves parallel to x-axis for 350 s. The actuator lengths and the rover body orientation are shown in Fig. 12. The actuator lengths

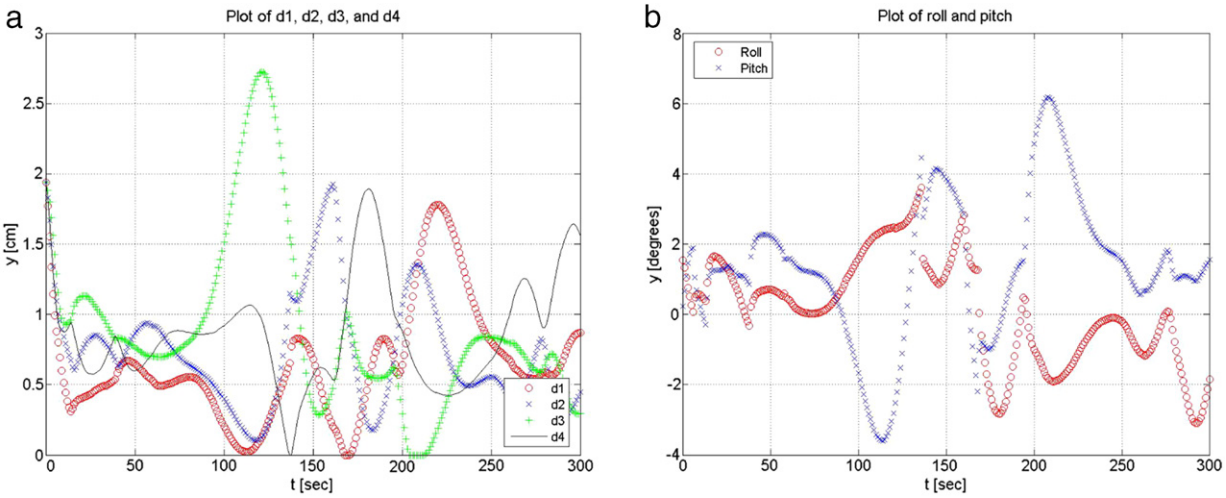

Fig. 14. (a) Actuator leg lengths and (b) rover body pitch and roll for the rough terrain.

d_2 and d_3 on the side that is wavy undergo substantial changes, i.e. from 0.5 to 6.0 cm whereas the actuators on the flat side, d_1 and d_4, change very little, as expected. The starting roll is 26°, which is quickly reduced to a range from 4° to 14°. In addition the pitch variation is small and ranges from −4° to 3.5°. These results indicate the correct behavior of the rover, as well as its optimization for a balanced operation.

Case 4. *Irregular rough terrain*.

The last case study is for a natural terrain shown in Fig. 13 which is a section of the JPL Mars yard. The original image was obtained from JPL and was processed to extract the topological information and produce Fig. 13 [24]. The rover starts at $(x, y) = (45, 410)$ cm and traverses on a straight path along a terrain diagonal and ends at $(320, 75)$ cm as shown in Fig. 13. The actuators lengths and the body roll/pitch angles are shown in Fig. 14. Each leg retracts or extends so as to conform to the complex terrain and to balance the rover. Despite the terrain bumps and ditches, the maximum roll angle is about 4° and the maximum pitch is about 6°. These demonstrate the versatile nature of the MTR in conforming to the terrain and the effectiveness of the actuation and balancing scheme.

In the final experiment the rover was required to traverse the terrain in Fig. 13 starting at along a path at $(x, y) = (40, 450)$ cm and moving on the line $y = 450$ cm. The rover now moves on a very bumpy part of the terrain. The actuator lengths (not shown) range from 0 to about 6 cm and pitch/roll (not shown) are within ±13° which are acceptable considering the challenging terrain.

5. Conclusions

A new methodology is presented for the kinematics modeling of high mobility rovers. The approach is very general and can be applied to any wheeled rover. It only requires setting up an extended DH table for the rover links and joints. The main feature of the work is its generality, e.g. dealing with both active (actuated) and passive (compliant) joints and linkages, and its ease of implementation. In particular, the proposed formulation makes the computer implementation very efficient. We have developed a computer program that reads the extended DH table of a rover and generates contact, navigation or actuation kinematics, as desired. Another contribution of the paper is the augmentation of a balance criterion into the kinematics of the rover. This allows determining actuations of various rover motors for path following while ensuring proper rover configuration for stability and tip over avoidance. The kinematics development and extended DH table construction have been performed for a high mobility rover with a complex mechanism. The results of applying the proposed method to this rover on several types of simulated terrains have been presented which demonstrate the ability to achieve balanced rover configurations when traversing rough terrain.

References

[1] P. Schenker, T. Huntsberger, P. Pirjanian, E. Baumgartner, E. Tunstel, Planetary rover developments supporting Mars exploration, sample return and future human robotic, colonization, Autonomous Robots 14 (2003) 103–126.
[2] R. Volpe, Rover functional autonomy development for Mars mobile science vehicles, in: Proc. IEEE Aerospace Conf., 2003, pp. 643–652.
[3] Y. Gonthier, E. Papadopoulos, On the development of a real-time simulator for and electro-hydraulic forestry machine, in: Proc. IEEE Int. Conf. Robotics & Automation, Leuven, Belgium, 1988.
[4] A.-J. Baerveldt (Ed.), Agricultural Robotics, in: Autonomous Robots, vol. 13-1, Kluwer Academic Publishers, 2002.
[5] J. Cunningham, J. Roberts, P. Corke, H. Durrant-Whyte, Automation of underground LHD and truck haulage, in: Proc. Australian IMM Conf., 1998, pp. 241–246.
[6] Ch. DeBolt, Ch. O'Donnell, S. Freed, T. Nguyen, The bugs 'basic UXO gathering system' project for UXO clearance and mine countermeasures, in: Proc. IEEE Int. Conf. Robotics and Automation, Albuquerque, NM, 1997, pp. 329–334.
[7] S. Sreenivasan, K. Waldron, Displacement analysis of an actively articulated vehicle configuration with extensions to motion planning on uneven terrain, Transactions of the ASME. Journal of Mechanical Design 118 (1996) 312–317.
[8] K. Iagnemma, S. Dubowski, Traction Control of wheel mobile robots in rough terrain with applications to planetary rovers, International Journal of Robotics Research 23 (10–11) (2003) 1029–1040.
[9] P.F. Muir, C.P. Neumann, Kinematic modeling of wheeled mobile robots, Journal of Robotic Systems 4 (2) (1987) 282–340.
[10] G. Campion, B. d'Andrea-Novel, Structural properties and classification of kinematic and dynamic models for wheel mobile robots, IEEE Transactions on Robotics and Automation 12 (1) (1996).
[11] B.J. Choi, S.V. Sreenivasan, Gross motion characteristics of articulated mobile robots with pure rolling capability on smooth uneven surfaces, IEEE Transactions on Robotics and Automation 15 (2) (1999) 340–343.
[12] M. Tarokh, G. McDermott, S. Hayati, J. Hung, Kinematic modeling of a high mobility Mars rover, in: Proc. IEEE Int. Conf. Robotics and Automation, Detroit, MI, 1999, pp. 992–998.
[13] M. Tarokh, G. McDermott, Kinematics modeling and analysis of articulated rovers, IEEE Transactions on Robotics 21 (4) (2005) 539–553.
[14] H.D. Nayar, I.A.D. Nesnas, Re-usable kinematics models and algorithms for manipulators and vehicles, in: Proc. IEEE/RSJ Int. Conf. Intelligent Robots and Systems, San Diego, 2007.
[15] J. Balaram, Kinematic observers for articulated rovers, in: Proc. IEEE Int. Conference on Robotics and Automation, San Francisco, CA, 2000, pp. 2597–2604.
[16] K. Iagnemma, S. Dubowski, Vehicle-ground contact angle estimation with application to mobile robot traction, in: Proc. 7th Int. Conf. on Advances on Robot Kinematics, Ark'00, 2000, pp. 137–146.
[17] K. Iagnemma, A. Rzepniewski, S. Dubowski, Control of vehicles with actively articulated suspension in rough terrain, Autonomous Robots 14 (2003) 5–16.
[18] G. McDermott, M. Tarokh, L. Mireles, Balance control of articulated rovers with active suspension systems, in: Proc. 7th IFAC Int. Conf. on Robot Control, vol. 8, Pt. 1, Italy, September 2006. Identifier: http://dx.doi.org/10.3182/20060906-3-IT-2910.00121.
[19] S. Nakamura, M. Faragalli, N. Mizukami, I. Nakatani, Y. Kunii, T. Kubota, Wheeled robot with movable center of mass for traversing over rough terrain, in: IEEE/RSJ Int. Conf. Intelligent Robots and Systems, San Diego, 2007.

[20] J. Craig, Introduction to Robotics, Mechanics and Control, Pearson, Prentice-Hall, 2005, pp. 144–146.
[21] N. Nakamura, Advanced Robotics-Redundancy and Optimization, Addison-Wesley, Boston, 1991 (Chapter 4).
[22] A.K. Bouloubasis, G.T. McKee, The mobility system of the multi-tasking rover (MTR), in: IEEE Int. Conf. Robotics and Automation, Rome, Italy, 2007.
[23] A.K. Bouloubasis, MTR the multi-tasking rover, http://www.youtube.com/watch?v=IMmJtw0XYzk, 2008.
[24] M. Tarokh, Hybrid intelligent path planning for articulated rovers in rough terrain, Fuzzy Sets and Systems 159 (21) (2008) 1–11. Elsevier.

Mahmoud Tarokh is a professor of computer science and the director of the Intelligent Machines and Robots Laboratory, Department of Computer Sciences, San Diego State University (SDSU), California, USA. Prior to joining SDSU he held academic positions at the University of California, San Diego, University of New Mexico and Sharif University of Technology, Iran. He has published extensively in the areas of robot path planning, rover kinematics, intelligent robotics system and robot control. He has conducted a number of research projects sponsored by government agencies and industries, notable among them National Aeronautics and Space Administration (NASA), Department of Defense, and National Science Foundation.

Huy Dang Ho received his B.S. degree in Computer Science from Assumption University, Thailand in 2005, and his M.S. degree in Computer Science from San Diego State University (SDSU), San Diego, CA in 2010. He is currently working at Webmetrics, a Neustar service, San Diego in the area of web performance monitoring, distributed and multi-agent systems. His research interests include kinematics modeling, machine learning and intelligent agents.

Antonios Bouloubasis received his Bachelor of Engineering (B.Eng.) in robotics and automated manufacturing from the University of Sussex in 2001, Masters in Cybernetics from University of Reading in 2002, and Ph.D. also from the University of Reading in 2008. In the same year, he co-founded 01 Mechatronics, a small automation company offering turn-key solutions for the industry and academia. Currently he is a senior structures and systems design engineer at Go Science, a company specializing in underwater robotic swarms for deep sea exploration. His area of expertise lies in systems design. He has developed the multi-tasking rover (MTR) a highly versatile rover which has various terrestrial and planetary applications. This work has resulted in several publications and has received recognition and awards.